Tassieri, M., Evans, R.M.L., Warren, R.L., Bailey, N.J., and Cooper, J.M. (2012) Microrheology with optical tweezers: data analysis. New Journal of Physics, 14 (11). p. 115032. ISSN 1367-2630

http://eprints.gla.ac.uk/72943/

Deposited on: 3 December 2012

Microrheology with optical tweezers: data analysis

Manlio Tassieri[1,4], R M L Evans[2], Rebecca L Warren[1], Nicholas J Bailey[3] and Jonathan M Cooper[1]

[1] Division of Biomedical Engineering, School of Engineering, University of Glasgow, Glasgow G12 8LT, UK
[2] Department of Applied Mathematics, University of Leeds, Leeds LS2 9JT, UK
[3] Centre for Music Technology, School of Engineering, University of Glasgow, Glasgow G12 8LT, UK
E-mail: Manlio.Tassieri@glasgow.ac.uk

Abstract. We present a data analysis procedure that provides the solution to a *long-standing* issue in microrheology studies, i.e. the evaluation of the fluids' linear viscoelastic properties from the analysis of a finite set of experimental data, describing (for instance) the time-dependent mean-square displacement of suspended probe particles experiencing Brownian fluctuations. We report, for the first time in the literature, the linear viscoelastic response of an optically trapped bead suspended in a Newtonian fluid, over the *entire* range of experimentally accessible frequencies. The general validity of the proposed method makes it transferable to the majority of microrheology and rheology techniques.

[4] Author to whom any correspondence should be addressed.

Contents

1. Introduction

Since their first appearance in the 1970s [1], optical tweezers (OT) have been extensively developed and have proved to be an invaluable tool for a variety of applications throughout the biophysical sciences: e.g. they have been successfully employed for measuring the microrheology of a colloidal suspension [2], the compliance of bacterial tails [3], the forces exerted by a single motor protein [4], the mechanical properties of human red blood cells [5] and those of individual biological molecules [6–8].

From a mechanical point of view, OT can be considered as exceptionally sensitive transducers able to resolve pN forces and nm displacements, with high temporal resolution (down to μs). The physics underpinning the working principles of the OT relies on the ability of a focused laser beam to trap, in three dimensions, micron-sized dielectric particles suspended in a fluid [1, 9, 10]. The trapping process is achieved by optically guiding a (monochromatic) laser beam through a high magnification objective, with high numerical aperture, which also allows visualization of the micro-environment surrounding the trapped probe. The trapping force is generated by the combined action of both the gradient of the laser intensity profile and the difference between the refractive indexes of the materials constituting the fluid and the probe. OT are very often built around optical microscopes, like those commonly used for biological studies, and are equipped with a fast probe-position detector. The latter is usually chosen to be either a charge-coupled device camera [11] or a quadrant photodiode [12]; both of which provide the tracer trajectory with a spatial resolution of the order of nm [13], but the first has a detection rate upper limit of the order of kHz, while the second can reach rates of the order of MHz. Accessing the time-dependent trajectory of a micron sphere, to high spatial and temporal resolution, is one of the basic principles behind microrheology techniques [14, 15], as introduced hereafter. For a fairly comprehensive review on the state of art of OT setups and their applications, we refer the reader to [16–22] and those therein.

Microrheology is a branch of rheology, but it works at micron length scales and with micro-litre sample volumes. Therefore, microrheology techniques are revealed to be very useful tools for all those rheological studies where rare or precious materials are employed

(e.g. in biomedical studies [23–25]). In addition, microrheology measurements can be performed *in situ* in an environment that cannot be reached by a bulk rheology experiment, for instance inside a living cell [26]. Microrheology techniques can be classified as either *passive* or *active*, depending on whether they monitor respectively the *free* or the *driven* motion of tracer particles introduced in the fluid under investigation. In the first case, the tracers' motion is governed by the thermal fluctuations of the surrounding fluid's molecules; whereas in the second case, an external force field is applied to the tracers. In the past decades, many microrheology techniques have been developed, including video particle tracking microrheology [27], diffusing wave spectroscopy [28, 29], atomic force microscopy [30], magnetic tweezers [31, 32] and OT [33–39]. For a good overview and understanding of the historical roots of the most common microrheology techniques, the reader is referred to [15, 40–42]. In general, microrheology techniques are aimed at relating the time-dependent tracers' trajectories to the linear viscoelastic (LVE) properties of the fluid in which they are dispersed.

The LVE properties of a material can be represented by the frequency-dependent complex shear modulus $G^*(\omega)$, which provides information on both the viscous and the elastic nature of the material. This is defined as the ratio between the Fourier transforms (denoted by the symbol '^') of the stress $\sigma(t)$ and the strain $\gamma(t)$ [43], regardless of which has been imposed and which has been measured:

$$G^*(\omega) = \frac{\hat{\sigma}(t)}{\hat{\gamma}(t)} \equiv \frac{\int_{-\infty}^{+\infty} \sigma(t) e^{-i\omega t}\, dt}{\int_{-\infty}^{+\infty} \gamma(t) e^{-i\omega t}\, dt}, \tag{1}$$

where ω is the angular frequency and i is the imaginary unit (i.e. $i^2 = -1$). The conventional method of measuring $G^*(\omega)$ is based on the imposition of an oscillatory stress $\sigma(\omega, t) = \sigma_0 \sin(\omega t)$ (where σ_0 is the amplitude of the stress function) and the measurement of the resulting oscillatory strain, which would have a form like $\gamma(\omega, t) = \gamma_0 \sin(\omega t + \delta(\omega))$, where γ_0 is the strain amplitude and $\delta(\omega)$ is the frequency-dependent phase shift between the stress and the strain; from equation (1) it follows that

$$G^*(\omega) = \frac{\sigma_0}{\gamma_0} \cos(\delta(\omega)) + i\frac{\sigma_0}{\gamma_0} \sin(\delta(\omega)) \equiv G'(\omega) + iG''(\omega), \tag{2}$$

where $G'(\omega)$ and $G''(\omega)$ represent the material storage (elastic) and loss (viscous) moduli, respectively. For example, in the case of a purely elastic solid, the stress and the strain are in phase and $\delta(\omega) = 0 \rightarrow G^*(\omega) \equiv G'(\omega)$; whereas, for a purely viscous fluid, such as water or glycerol, $\delta(\omega) = \pi/2 \rightarrow G^*(\omega) \equiv iG''(\omega)$. For complex solids (e.g. gels, rubbers) or viscoelastic fluids (e.g. oil [44], saliva [45]) $\delta(\omega)$ would take any value between the above limits (i.e. $0 \leqslant \delta(\omega) \leqslant \pi/2$) depending on the frequency at which the stress or the strain is applied. Note that $G^*(\omega)$ is time invariant.

In this paper we provide the solution to a *long-standing* issue in microrheology studies, i.e. the evaluation of the fluids' LVE properties from the analysis of a finite set of experimental data, describing (for instance) the time-dependent mean-square displacement (MSD) of suspended probe particles experiencing Brownian fluctuations [14, 46–53]. In particular, we *tune* the analytical method introduced by Evans *et al* [54], for converting creep compliance $J(t)$ (a function simply proportional to the MSD) into $G'(\omega)$ and $G''(\omega)$, to microrheology measurements performed with OT. We report, for the first time in the literature, the LVE response of an optically trapped bead suspended in a Newtonian fluid, over the *entire* range of experimentally accessible frequencies; both for synthetic and real experimental data. In addition, we present an improved method to evaluate the frequency-dependent complex shear modulus

$G^*(\omega)$ of generic fluids including water-based solutions of F-actin protein. The general validity of the proposed method makes it transferable to the majority of microrheology techniques.

The paper is organized as follows. In section 2 we describe the apparatus used. In section 3, we discuss the theoretical background required to obtain rheological data from OT. In section 4, we discuss novel methods of data analysis that avoid the introduction of artefacts. We anticipate some results for a relevant biological fluid (i.e. solutions of actin filaments) in section 5, and draw conclusions in section 6.

2. Apparatus

Optical trapping is achieved by means of a titanium-sapphire laser with a 5 W pump (Verdi V5 laser; Coherent Inc.), which provides up to 1 W at 830 nm. The tweezers are based around an inverted microscope, where the same objective lens (100×, 1.3 numerical aperture, Zeiss, Plan-Neofluor) is used both to focus the trapping beam and to image the thermal fluctuations of either a 2 or 5 μm diameter silica bead. Samples are mounted on a motorized microscope stage (Prior Pro-Scan II). A complementary metal-oxide semiconductor camera (Dalsa Genie HM640 GigE) takes high-speed images of a reduced field of view. These images are processed in real-time at ≈1 kHz using our own LabVIEW (National Instruments) particle tracking software [55] running on a standard personal computer.

3. Theoretical background

When a micron-sized spherical particle is suspended in a fluid at thermal equilibrium, it experiences random forces leading to Brownian motion, driven by the thermal fluctuations of the fluid's molecules. Analysis of the particle's trajectory reveals information on the viscoelastic properties of the suspending fluid, as demonstrated in the pioneering work of Mason and Weitz [14] that established the field of microrheology. In particular, they showed that, at thermal equilibrium, the trajectory $\vec{r}(t) \, \forall \, t$ of a naturally buoyant bead is directly related to the LVE properties of the surrounding complex fluid by means of a generalized Langevin equation

$$m\vec{a}(t) = \vec{f}_R(t) - \int_0^t \zeta(t-\tau)\vec{v}(\tau)\,\mathrm{d}\tau, \tag{3}$$

where m is the mass of the particle, $\vec{a}(t)$ is its acceleration, $\vec{v}(t)$ its velocity and $\vec{f}_R(t)$ is the usual Gaussian white noise term, modelling stochastic thermal forces acting on the particle. The integral term, which incorporates a generalized time-dependent memory function $\zeta(t)$, represents viscous damping by the fluid. Using the assumption that the Laplace-transformed bulk viscosity of the fluid $\tilde{\eta}(s)$ is proportional to the microscopic memory function $\tilde{\zeta}(s) = 6\pi a\tilde{\eta}(s)$, where a is the bead radius, they provided the solution to equation (3) in terms of the MSD:

$$G^*(\omega) = s\tilde{\eta}(s)|_{s=\mathrm{i}\,\omega} = \frac{1}{6\pi a}\left[\frac{6k_\mathrm{B}T}{\mathrm{i}\,\omega\langle\Delta\widehat{r^2}(\omega)\rangle} + m\omega^2\right], \tag{4}$$

where k_B is Boltzmann's constant, T is absolute temperature and $\langle\Delta\widehat{r^2}(\omega)\rangle$ is the Fourier transform of the MSD $\langle\Delta r^2(\tau)\rangle \equiv \langle[\vec{r}(t+\tau) - \vec{r}(t)]^2\rangle$. The average $\langle\ldots\rangle$ is taken over all initial times t and all particles, if more than one is observed.

IOP Institute of Physics Φ DEUTSCHE PHYSIKALISCHE GESELLSCHAFT

In the case when the probe's fluctuations are constrained by a stationary harmonic potential generated by OT, one could write a generalized Langevin equation similar to equation (3), but with an additional term accounting for the trapping force:

$$m\vec{a}(t) = \vec{f}_R(t) - \int_0^t \zeta(t-\tau)\vec{v}(\tau)\,\mathrm{d}\tau - \kappa\vec{r}(t). \tag{5}$$

Here, κ is the OT trap stiffness, which can be easily determined by appealing to the principle of equipartition of energy:

$$\frac{d}{2}k_\mathrm{B}T = \frac{1}{2}\kappa\langle r_j^2 \rangle, \tag{6}$$

where $\langle r_j^2 \rangle$ is the time-independent variance of the Cartesian component ($j = x, y, z$) of the d-dimensional vector describing the particle's displacement from the trap centre, the origin of $\vec{r}$. Note that, for non-symmetric traps (i.e. $\kappa \neq \kappa_j$, $\forall j$) equation (5) is still valid but in one dimension, with κ replaced by κ_j evaluated for each component. Despite the great variety of methods for determining the trap stiffness (e.g. using the power spectrum or the drag force [18, 56, 57]), equation (6) provides the only such measurement that is independent of the viscoelastic properties of the fluid under investigation and is thus essential for proper calibration. This is because, whatever the elasticity of the unknown fluid, its contribution to the time-independent constraining force must vanish at long lag-times (because at rest the fluid's elastic shear modulus goes to zero as the time goes to infinity). Thus the trap stiffness is easily determined by means of equation (6) applied to a *sufficiently long measurement* (i.e. longer than the fluid's longest relaxation time) via the evaluation of the time-independent variance of the confined particle position.

Following the same assumptions made by Mason and Weitz for the case of freely diffusing particles, equation (5) can be solved in terms of either the normalized mean-square displacement (NMSD) $\Pi(\tau) = \langle \Delta r^2(\tau)\rangle/2\langle r^2\rangle$ [36] or the normalized position autocorrelation function (NPAF) $A(\tau) = \langle \vec{r}(t)\vec{r}(t+\tau)\rangle/\langle r^2\rangle$ [37]:

$$G^*(\omega)\frac{6\pi a}{\kappa} = \left(\frac{1}{\mathrm{i}\,\omega\hat{\Pi}(\omega)} - 1\right) \equiv \left(\frac{1}{\mathrm{i}\,\omega\hat{A}(\omega)} - 1\right)^{-1}, \tag{7}$$

where $\hat{\Pi}(\omega)$ and $\hat{A}(\omega)$ are the Fourier transforms of $\Pi(\tau)$ and $A(\tau)$, respectively. The inertial term ($m\omega^2$), present in the original publications [36, 37], has been neglected here because, for micron-sized particles, it only becomes significant above the MHz frequency range. The quantities $A(\tau)$ and $\Pi(\tau)$ are simply related to each other [37]:

$$\Pi(\tau) \equiv \frac{\langle r^2(t+\tau)\rangle + \langle r^2(t)\rangle - 2\langle \vec{r}(t_0)\vec{r}(\tau)\rangle}{2\langle r^2\rangle} \equiv 1 - A(\tau). \tag{8}$$

In addition, by Fourier transforming equation (8) one obtains the relation: $\mathrm{i}\,\omega\hat{\Pi}(\omega) = 1 - \mathrm{i}\,\omega\hat{A}(\omega)$, which will prove useful later in the manuscript. The relationships between measurements made in the presence or absence of an OT are further reviewed in the appendix.

In principle, equations (4) and (7) are simple expressions relating the material's complex shear modulus $G^*(\omega)$ to the observed time-dependent bead trajectory $\vec{r}(t)$ via the Fourier transform of one of the related time-averaged quantities. In practice, the evaluation of these Fourier transforms, given only a finite set of data points over a finite time domain, is non-trivial since interpolation and extrapolation from those data can yield artefacts that lie within the bandwidth of interest.

The first attempt to address this issue for microrheology [14] was to fit the measured $\tilde{G}(s)$ to a preconceived functional form, and then use analytic continuation (swapping Laplace for Fourier frequency, $s \rightarrow i\omega$) to recover $G'(\omega)$ and $G''(\omega)$. A later approximate method [51] recovered the moduli from the log slope of the MSD, without numerical inversions, and was subsequently improved upon [52] by accounting for curvature.

An alternative method has been proposed by Evans *et al* [54] to convert creep compliance $J(t)$ (and therefore MSD) into $G'(\omega)$ and $G''(\omega)$ directly, without transforms or fitting functions. This method is based on the interpolation of the finite data set by means of a piecewise-linear function. The general validity of the proposed procedure makes it equally applicable to find the Fourier transform $\hat{g}(\omega)$ of any time-dependent function $g(t)$ that vanishes for negative t, sampled at a finite set of data points (t_k, g_k), where $k = 1, \ldots, N$, which extend over a finite range, and *need not* be equally spaced [54]:

$$-\omega^2 \hat{g}(\omega) = i\,\omega g(0) + (1 - e^{-i\omega t_1})\frac{(g_1 - g(0))}{t_1} + \dot{g}_\infty e^{-i\omega t_N} + \sum_{k=2}^{N} \left(\frac{g_k - g_{k-1}}{t_k - t_{k-1}}\right)(e^{-i\omega t_{k-1}} - e^{-i\omega t_k}),$$

(9)

where $\dot{g}_\infty$ is the gradient of $g(t)$ extrapolated to infinite time and $g(0)$ is the value of $g(t)$ extrapolated to $t = 0$ from above.

4. Data analysis

Although equation (9) has been successfully employed in both classical bulk rheology [58, 59] and microrheology studies [32, 36, 37, 53], when it is applied to microrheology measurements performed with OT, there remain *two* issues, common to all the other methods described above, that compromise the quality of the results. Nevertheless, we shall introduce a data analysis procedure that markedly reduces the undesired effects of these experimental issues, providing a useful tool for microrheology.

4.1. Interpolation artefacts

The first issue is related to the Nyquist–Shannon sampling theorem [60]: '*If a function contains no frequencies higher than W cps, it is completely determined by giving its ordinates at a series of points spaced* $1/(2\,W)$ *seconds apart*'. Conversely, we cannot expect to recover complete information about the fluid's LVE properties from the Fourier transform of a discrete data set (e.g. MSD, NMSD or NPAF) at frequencies higher than one half of the data acquisition rate (AR) if the rate is uniform. Above that frequency, the information in the Fourier transform is artificial, describing the details of the interpolation scheme between the data points. Unfortunately, those artefacts will almost certainly spread some way *below* the Nyquist limit, contaminating the experimental results. This occurs due to the broad spectrum of the sharp corners between straight-line segments in the interpolation scheme used to derive equation (9).

This first issue is simply resolved by *virtually* oversampling the time-averaged functions (e.g. $\Pi(\tau)$) that contain the fluid's LVE properties. Oversampling is a very common procedure in signal processing and it consists of sampling a signal with a sampling frequency f_s much higher than the Nyquist rate $2B$, where B is the highest frequency contained in the original signal. A signal is said to be oversampled by a factor of $\beta \equiv f_s/(2B)$ [61]. Microrheological

measurements performed with OT have a maximum value of B limited by the detector's AR. We choose to oversample by interpolating the measured time-averaged functions (e.g. $A(\tau)$) with a natural cubic spline, which is piecewise cubic and twice continuously differentiable.

Having generated the larger over-sampled data set from the original data set, it remains important to use equation (9) to find its Fourier transform, since that equation correctly assumes causality (the function vanishes for negative time), extrapolates to infinite time (using the parameter $\dot{g}_\infty$) and guarantees that no other assumptions bias the data. In contrast to our cubic-spline interpolation, a fitting procedure based on preconceived models would *doctor* the experimental results; our interpolation procedure preserves the original data within the bandwidth limits imposed by the sample rate. Note that, following the oversampling and conversion, the resulting rheological data (the frequency-dependent viscoelastic moduli) should only be examined at frequencies within the experimentally valid frequency window, since no real information exists above the Nyquist frequency. We shall show that this data-analysis procedure yields artefact-free results right up to the Nyquist limit.

To validate the solution to this first issue, we initially apply it to a simple analytical example NPAF, in the form of a single exponential decay: $A(\tau) = e^{-\lambda\tau}$, where $\lambda = \kappa/(6\pi a \eta)$, as if obtained from infinitely long measurements of the thermal fluctuations of a particle harmonically trapped in a Newtonian fluid. This is the dynamic response of an ideal Kelvin–Voigt material (see equation (A.6)), for which the frequency spectrum is known to have a simple analytical form (equation (A.7)). Defining the normalized complex modulus $\bar{G}^*_{\text{tot}}(\omega) \equiv (6\pi a/\kappa)\, G^*_{\text{tot}}(\omega)$ and substituting the Kelvin–Voigt NPAF into equation (7) yields

$$\bar{G}^*_{\text{tot}}(\omega) = 1 + i\,\bar{\omega}, \tag{10}$$

where $\bar{\omega} = \omega/\lambda$.

In figure 1 (left) we report an example in which the idealized NPAF has been sampled at a frequency of $f_s = 1\,\text{kHz}$, as if it were obtained from thermal fluctuations of a $5\,\mu\text{m}$ diameter sphere constrained by an OT with trap stiffness of $\kappa = 1\,\mu\text{N m}^{-1}$ and suspended in a Newtonian fluid of viscosity $\eta = 0.896\,\text{mPa s}$, where the bead trajectory had been acquired at $\text{AR} \equiv f_s$ and for an infinite time, up to a lag-time of 1 s. We reconstruct the dynamic response of the system via equation (A.6), with the Fourier transform of $A(\tau)$ evaluated by means of equation (9); the results are shown in figure 1 (right). It is clear that artefacts in the frequency domain, where $\bar{G}'_{\text{tot}}(\omega)$ starts to diverge from its expected value (due to the finite sampling rate and implicit piecewise-linear interpolation in the time domain), begin at $\omega \simeq \lambda$ (i.e. $\bar{\omega} \simeq 1$), whereas, $\bar{G}''_{\text{tot}}(\omega)$ starts to deviate from its expected value (i.e. $\bar{\omega}$) only at $\omega \simeq 20\lambda$.

Figure 2 demonstrates that the correct values of the LVE moduli are recovered by oversampling the discrete data shown in figure 1 (left) to a sufficiently high value of $\beta \equiv f_s/(2\text{AR}) \gg \omega/\text{AR}$, using a natural cubic spline interpolation. Here, we have taken $f_s \cong 8.2\,\text{MHz}$, implying $\beta \cong 4100$. Note that a detailed study of the errors in evaluating the moduli as a function of β is reported in the appendix. In figure 2, both the moduli now show the expected values (i.e. equation (10)) over the *entire* range of explored frequencies.

4.2. Noise

The second issue relates to the accuracy with which the data (i.e. $\langle \Delta r^2(\tau) \rangle$, $\Pi(\tau)$ or $A(\tau)$) are evaluated, especially at long lag-times. Indeed, since all the functions of particle position
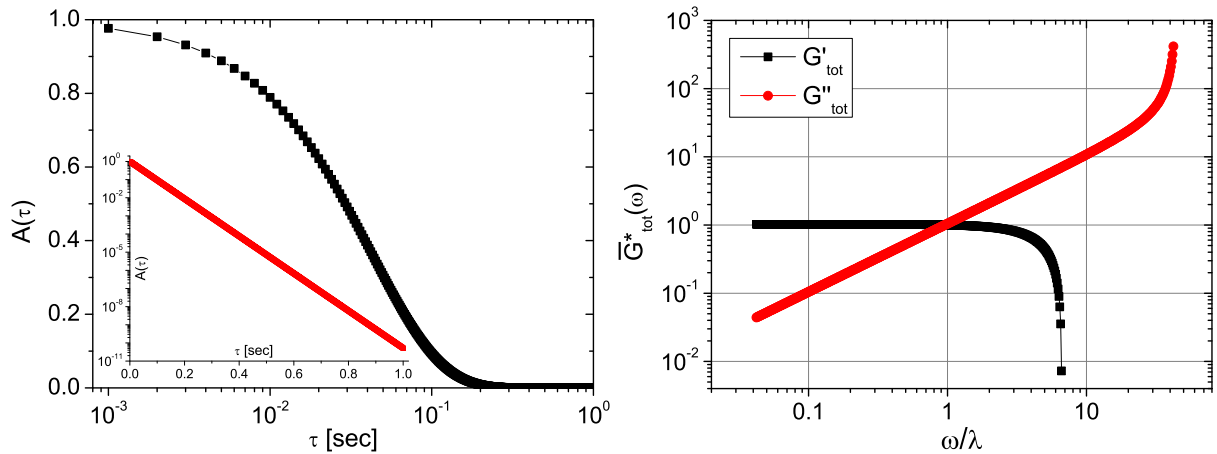
Figure 1. (Left) The NPAF $(A(\tau) = e^{-\lambda\tau})$ versus lag-time, where $\lambda = \kappa/(6\pi a\eta) \simeq 24\,\text{s}^{-1}$. The NPAF has been built using the following parameter values: $f_s = 1\,\text{kHz}$, $\kappa = 1\,\mu\text{N}\,\text{m}^{-1}$, $a = 2.5\,\mu\text{m}$, $\eta = 0.896\,\text{mPa}\,\text{s}$. The inset shows the same data as above, but with the semi-log representation of the axis inverted. (Right) The normalized complex modulus versus frequency evaluated via equation (7) and by means of equation (9) applied to the data shown on the left; both quantities are dimensionless.
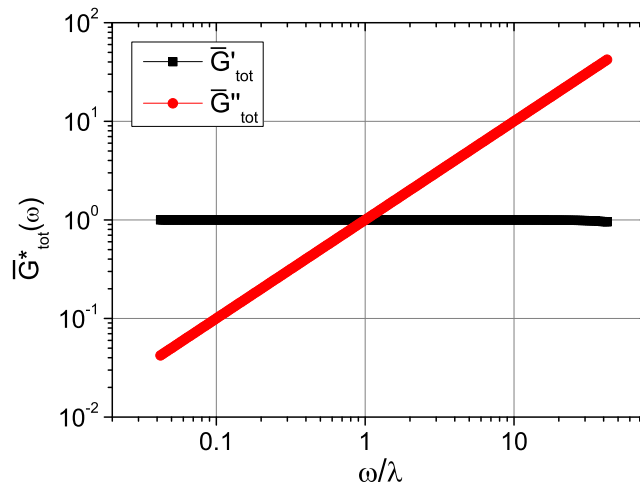

Figure 2. The normalized complex modulus versus frequency evaluated via equation (7) and by means of equation (9) applied to the data shown in figure 1 (left), but interpolated with a natural cubic spline function having $f_s \cong 8.2\,\text{MHz}$. This correct normalization confirms the validity of the data analysis method.

in equations (4) and (7) are time-averaged quantities, they become *exact* only in the limit of infinite measuring time (or equivalently for $N \to \infty$), which is unachievable in reality.

In order to quantify the uncertainty of a time-averaged function (measured over a finite set of data) with respect to its expected value, we have evaluated the MSD of 10^4 simulated trajectories of freely diffusing particles, with each trajectory comprising 10^6 random steps,
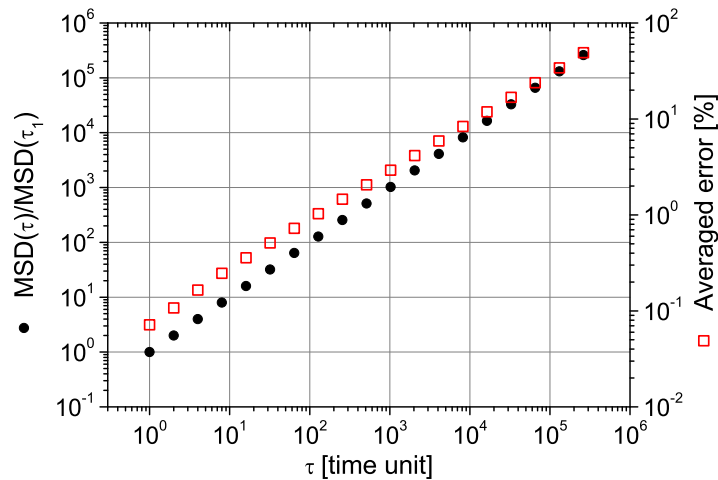
Figure 3. (Left axis) The MSD versus lag-time of 10^4 simulated trajectories of freely diffusing particles; each trajectory is made up by 10^6 data points (i.e. steps). (Right axis) The percentage deviation of the MSD from its expected value for each trajectory.

drawn from a uniform distribution of unit width; so that, e.g. the MSD at lag-time $\tau = 1$ has been evaluated over $\sim 10^{10}$ displacements. The resulting curve shown in figure 3 satisfies the expectation that MSD $\propto \tau$. However, within a single trajectory of 10^6 steps the error in the measured MSD, for a lag-time of 10^4 time units is typically as large as 10%. As shown in figure 3, the percentage deviation of the MSD(τ) from its expected value for each trajectory grows with lag-time, as a power law close to $\tau^{1/2}$.

In real experiments this uncertainty affects the results in the following way. Since the Fourier transform is an integral operator, all the short time-scale deviations of the measured time-averaged function from its expected value will communally contribute noise to the results at high frequencies, especially those occurring at long lag-times where the averages are inexorably less accurate. This is clearly shown in figure 4 (left), where the agreement between the measured NMSD and its prediction, via equation (A.5), is very good at small lag-times; whereas it becomes worse at long lag-times (see the inset of figure 4 (left)). Although *all* of the data contribute to the high-frequency *noise*, the high-frequency *signal* derives predominantly from the measurements at short lag-times. In long-duration experiments, this signal can become swamped by noise from the large quantity of long lag-time data. A simple but crude solution to this problem, to improve the signal-to-noise ratio, is obtained by reducing the data density (i.e. the sampling rate) at long lag-times. This is achieved by evaluating the time-averaged functions (e.g. $A(\tau)$) at values of τ that are logarithmically (or near-logarithmically) distributed on the time-scale, as shown in figure 4 (right). In this particular case, we have evaluated (or sampled) $A(\tau)$ at lag-times $\tau_n = \mathrm{ceil}(1.45^n)$, for non-negative integer n (where ceil(...) is the ceiling function, which rounds the input variable to the next highest integer); so that, the first five points are linearly spaced in time, whereas all the others are logarithmically distributed. In this way, we enhance the relative statistical weight of the reliable data at short lag-times and substantially reduce the number of disruptive short time-scale deviations of $A(\tau)$ from its expected value, occurring at long lag-times.
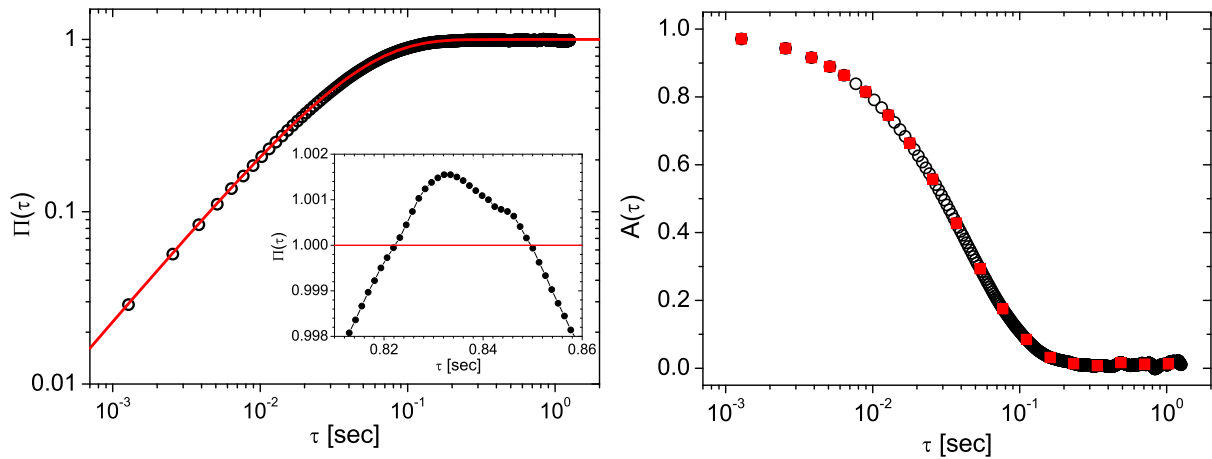
Figure 4. (Left) Comparison between the $\Pi(\tau)$ (circles) and its prediction (continuous line), via equation (A.5), for an optically trapped 4.74 μm diameter silica bead suspended in water, with $\kappa = 0.93 \, \mu\mathrm{N}\,\mathrm{m}^{-1}$ and $\eta = 0.896 \, \mathrm{mPa}\,\mathrm{s}$. The NMSD has been obtained from the analysis of 10^6 data points representing the particle trajectory, acquired at AR $\simeq 1$ kHz. The inset highlights the behaviour of $\Pi(\tau)$ within a small time-window taken at long lag-times. (Right) The same data as shown on the left, but plotted in terms of the NPAF versus lag-time (circles); whereas the red square symbols represent the same data as before, but sampled at lag-times quasi-logarithmically distributed on the time-scale: $\tau_n = \mathrm{ceil}(1.45^n)$, for non-negative integer n.

Finally, we apply both the above techniques to analyse real experimental data, to yield the full viscoelastic spectrum of optically trapped micro-spheres suspended in Newtonian fluids. In figure 5 (left) we report the NPAF of optically trapped spheres suspended in both water and 20% w/w glycerol/water mixture while, in figure 5 (right), we report the real and imaginary parts of the normalized complex modulus evaluated via equation (A.6) and by means of equation (9) applied to the sampled data shown in figure 5 (left) after interpolation with a natural cubic spline function having $f_\mathrm{s} = 25$ and $\simeq 3.7$ MHz, respectively. From figure 5 (right) it is clear that, although there remains some noise in the real component of the complex modulus at high frequencies, the agreement between the results and the expected values (i.e. equation (10)) is very good.

Based on these results, we can confirm that the OT acts as a linear force transducer when operating in the range of frequencies up to ∼kHz and on micron-sized particles (i.e. when the laser wavelength is smaller than the particle diameter). However, it is important to be aware that, under other operating conditions, the OT response may not remain linear [62–65].

5. Results for solutions of actin filaments

Having established the efficacy of the new method of data analysis, we use it to obtain clean, artefact-free viscoelastic moduli of an important biological fluid, for which conventional rheology is difficult due to the sample volumes available. In particular, we anticipate some results from an OT based microrheology study performed on solutions of actin filaments, reminding that more detailed bio-physical studies of these solutions will be presented elsewhere.
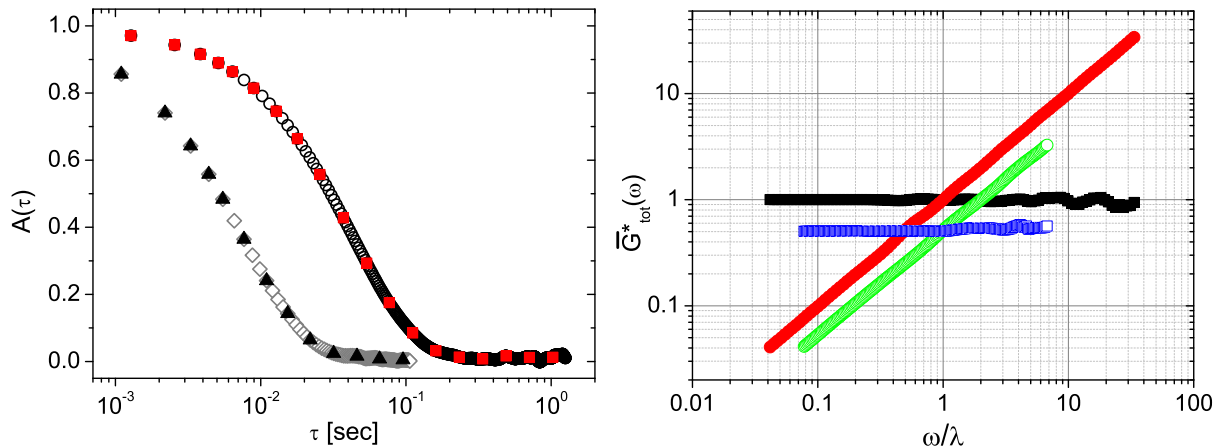
Figure 5. (Left) Comparison between the NPAF shown in figure 4 (circles) with that obtained from the analysis of an optically trapped $2\,\mu$m diameter silica bead suspended in 20% w/w glycerol/water mixture (diamonds), with $\kappa = 4\,\mu$N m^{-1} and $\eta = 1.6\,$mPa s. Both the NPAFs have been sampled at lag-times quasi-logarithmically distributed on the time-scale: $\tau_n = \mathrm{ceil}(1.45^n)$, for non-negative integer n (squares and triangles, respectively). (Right) The normalized complex modulus versus frequency (both dimensionless) evaluated via equation (7) and by means of equation (9) applied to the sampled NPAFs shown on the left, but interpolated with a natural cubic spline function having $f_s = 25$ and $\simeq 3.7\,$MHz, respectively. Note that, the normalized moduli obtained from the glycerol/water mixture (i.e. $\bar{G}'$, blue open square symbols, and $\bar{G}''$, green open circle symbols) have been scaled by a factor of two for a clearer visualization. The black square and the red circle symbols represent the normalized moduli for the measurement performed with water.

The cytoskeleton is a network of protein-fibres that runs throughout the matrix of living cells. It provides a framework for organelles, anchors the cell membrane, facilitates cellular movement and provides a suitable surface for chemical reactions to occur. The cytoskeleton is made up of three types of protein filaments: microfilaments (also called thin filaments), intermediate filaments and microtubules. The mechanical properties of thin filament networks control specific biological functions (e.g. regulation of muscle contraction), but these mechanical properties are difficult to measure *in vivo*. This problem has motivated an extensive research effort to investigate the mechanical properties and microstructure of reconstituted thin filament networks *in vitro* [66–69]. At low ionic strength *in vitro*, actin exists in the monomeric (globular) G-actin form. G-actin is roughly spherical with a diameter of about 5 nm. When the ionic strength of a G-actin solution is increased to a physiological value (0.1 M), G-actin self-associates to form the backbone of the thin filament—the actin filament (F-actin), which can be viewed as either a two-stranded long-pitch ($\simeq 37$ nm) helical structure or a single short-pitch ($\simeq 5.9$ nm) helical structure [70], which is related to the size of the monomeric G-actin.

F-actin is a biological example of a semi-flexible polymer that is characterized by a persistence length ranging from ~ 2 to $\sim 30\,\mu$m [71–73] and a diameter of $\simeq 8$ nm [71, 74]. Despite their importance to biophysical studies, the viscoelastic properties of semi-flexible polymer solutions are still not well understood and a basic analytical model has not yet been
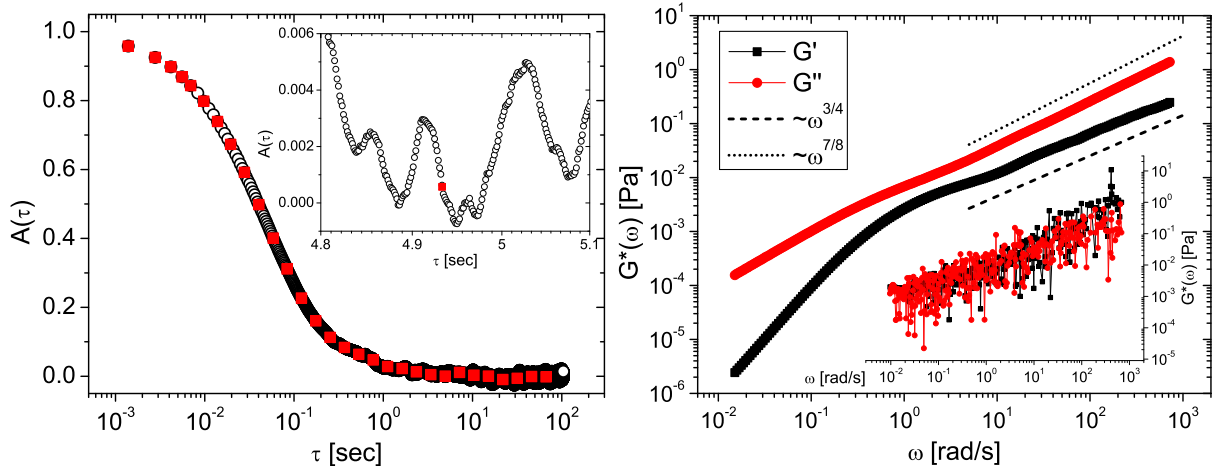
Figure 6. (Left) (Circles) The NPAF versus lag-time of an optically trapped $5\,\mu$m diameter silica bead suspended in a solution of F-actin at concentration of $0.1\,\mathrm{mg\,ml^{-1}}$ and $\kappa = 2.8\,\mu\mathrm{N\,m^{-1}}$. The NPAF has been evaluated from a trajectory made up by 10^6 data points. (Squares) Same data as before, but sampled at lag-times quasi-logarithmically distributed on the time-scale: $\tau_n = \mathrm{ceil}(1.45^n)$, for non-negative integer n. The inset shows the disruptive short time-scale deviations occurring at long lag-times. (Right) The complex modulus versus frequency evaluated via equation (7) and by means of equation (9) applied to the sampled NPAF shown on the left, but interpolated with a natural cubic spline function having $f_s = 12\,\mathrm{MHz}$. The lines are guides for the gradients. The inset shows the disruptive effects of the short time-scale deviations occurring at long lag-times when the $G^*(\omega)$ is evaluated via equation (7) and by means of equation (9) directly applied to the original NPAF shown on the left.

agreed upon; thus the need of accurate experimental data describing the rheological properties of semi-flexible polymer solutions to inform the development of theoretical models.

In figure 6 (left) we report the NPAF of an optically trapped $5\,\mu$m diameter silica bead suspended in a solution of F-actin at concentration of $0.1\,\mathrm{mg\,ml^{-1}}$. The inset shows the short time-scale deviations occurring at long lag-times because of the poor accuracy to which $A(\tau)$ can be evaluated from a finite-size data set representing the particle trajectory $\vec{r}(t)$ (here 10^6 data points). Figure 6 (right) shows the LVE properties of the F-actin solution evaluated via equation (7) and by means of equation (9) applied to the sampled $A(\tau)$ after interpolation with a natural cubic spline function with $f_s = 12\,\mathrm{MHz}$. At high frequencies, both moduli are in good agreement with the theoretical predictions: $G'(\omega) \propto \omega^{3/4}$ and $G''(\omega) \propto \omega^{7/8}$. Indeed, while the former power-law is an archetype for the dynamics of semi-flexible polymer solutions [75, 76], the latter is not so commonly observed, although predicted by Everaers *et al* [77], Liverpool [78] and, more recently [79, 80], in models that combine the effects of both longitudinal and transverse fluctuations on the dynamics of a semi-flexible filament. They found that, at short times, the fluctuations perpendicular to the local axis of the polymer scale as $\langle r_\perp^2 \rangle \propto t^{3/4}$ (similarly found by Morse [76]), while fluctuations parallel to the local axis follow a different law $\langle r_\parallel^2 \rangle \propto t^{7/8}$ and are correlated over a length $l_\parallel \propto t^{1/8}$.

6. Conclusions

An improved data analysis procedure for determining the LVE properties of complex fluids has been successfully applied to microrheology measurements with OT. The reliability of the *novel* data analysis procedure has been tested by evaluating the LVE response of optically trapped beads suspended in Newtonian fluids. For the first time in the literature, the frequency-independent elastic component of an optical trap has been measured over the *entire* range of experimentally accessible frequencies. The general validity of the proposed method makes it transferable to the majority of microrheology and rheology techniques.

Appendix A. Rheological characterization of optical tweezers

It is worthwhile reviewing some fundamental relationships between the most common parameters describing the materials' LVE properties and the time-averaged functions (e.g. MSD) derived by analysis of the particle's thermal fluctuations. Let us begin by describing a simple relationship between the MSD of a freely diffusing particle and the time-dependent compliance $J(t)$ of the suspending fluid. In classical rheology (i.e. in shear flow), the creep compliance is defined as the ratio of the time-dependent shear strain $\gamma(t)$ to the magnitude σ_0 of the constant shear stress that is switched on at time $t = 0$: $J(t) = \gamma(t)/\sigma_0$. The latter is related to the shear relaxation modulus $G(t)$ by a convolution [43]

$$\int_0^t G(\tau)\, J(t - \tau)\, \mathrm{d}\tau = t. \tag{A.1}$$

Since the complex shear modulus $G^*(\omega)$ (i.e. equation (1)) is the Fourier transform of the time derivative of $G(t)$, by taking the Fourier transform of equation (A.1) it follows that

$$G^*(\omega) = \mathrm{i}\,\omega \hat{G}(\omega) = \frac{1}{\mathrm{i}\,\omega \hat{J}(\omega)}, \tag{A.2}$$

where $\hat{G}(\omega)$ and $\hat{J}(\omega)$ are the Fourier transforms of $G(t)$ and $J(t)$, respectively. By equating equations (A.2) and (4) one obtains

$$\langle \widehat{\Delta r^2}(\omega) \rangle = \frac{k_\mathrm{B} T}{\pi a} \hat{J}(\omega) \Longleftrightarrow \langle \Delta r^2(\tau) \rangle = \frac{k_\mathrm{B} T}{\pi a} J(t), \tag{A.3}$$

where it has been assumed that the inertial term $(m\omega^2)$ in equation (4) is negligible for frequencies $\ll$ MHz and that $J(0) = 0$ for viscoelastic fluids. Equation (A.3) expresses the linear relationship between the MSD of suspended spherical particles and the macroscopic creep compliance of the suspending fluid [81].

Let us now consider an optically trapped spherical particle suspended in a viscoelastic fluid. For such a system, equation (A.3) would still hold, but it would describe the relationship
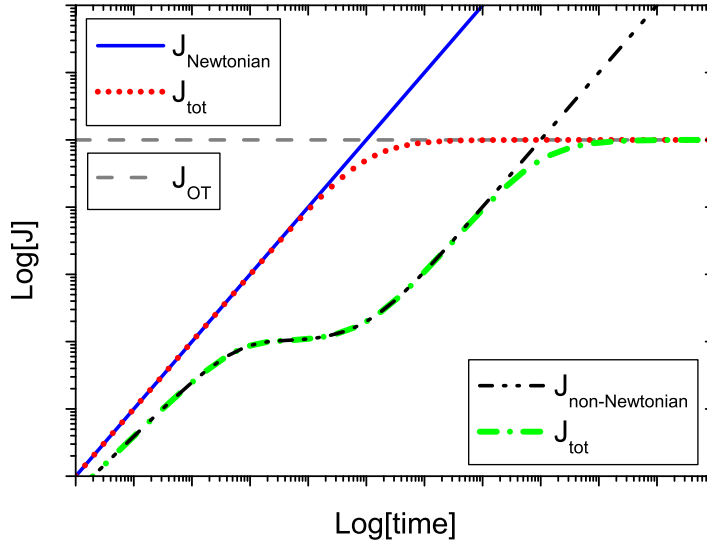
Figure 7. Schematic representations of $J_{\text{tot}}(t)$ ($\propto \Pi(\tau)$, see equation (A.4)) for the cases of a trapped spherical particle suspended in both a Newtonian fluid and a generic viscoelastic fluid.

between the measured MSD of a constrained particle and the compliance (J_{tot}) of the compound system made up of the optical trap and the viscoelastic fluid:

$$\left\langle \Delta r^2(\tau) \right\rangle = \frac{k_{\text{B}}T}{\pi a} J_{\text{tot}}(t) \quad \text{or} \quad \Pi(\tau) = \frac{\kappa}{2d\pi a} J_{\text{tot}}(t), \tag{A.4}$$

where the second expression follows from equations (6) and (8). In the simplest case where $\kappa \equiv \kappa_j \forall j$ ($j = x, y, z$), $d = 3$ and the suspending fluid is Newtonian, with a time-independent viscosity η, the compound system (OT plus fluid) can be modelled as an *ideal* Kelvin–Voigt material, with elastic constant proportional to the trap stiffness, $\kappa/(6\pi a)$, and viscosity equal to η. In this case, J_{tot} assumes a simple analytical form

$$J_{\text{tot}} = \frac{6\pi a}{\kappa} \left(1 - e^{-\lambda t} \right) \Rightarrow \Pi(\tau) = \left(1 - e^{-\lambda \tau} \right), \tag{A.5}$$

where $\lambda = \kappa/(6\pi a\eta)$ is the relaxation rate of the compound system, known as the *corner frequency* when the thermal fluctuations of an optically trapped bead are analysed in terms of the power spectral density [56]. In practice, λ defines a characteristic time ($t^* = \lambda^{-1}$) at which the fluid compliance ($J(t) = t/\eta(t)$) equals the compliance of the optical trap ($J_{\text{OT}} = 6\pi a/\kappa$): $J(t^*) = J_{\text{OT}}$; as schematically shown in figure 7, where the intersection of $J(t)$ and J_{OT} identifies t^*.

Finally, from equations (A.2) and (A.4), one can also express the viscoelastic properties of the compound system in the frequency domain:

$$G_{\text{tot}}^*(\omega) = \frac{\kappa}{6\pi a} \frac{1}{\mathrm{i}\,\omega\hat{\Pi}(\omega)} \tag{A.6}$$

which, for a system modelled as an *ideal* Kelvin–Voigt material, becomes

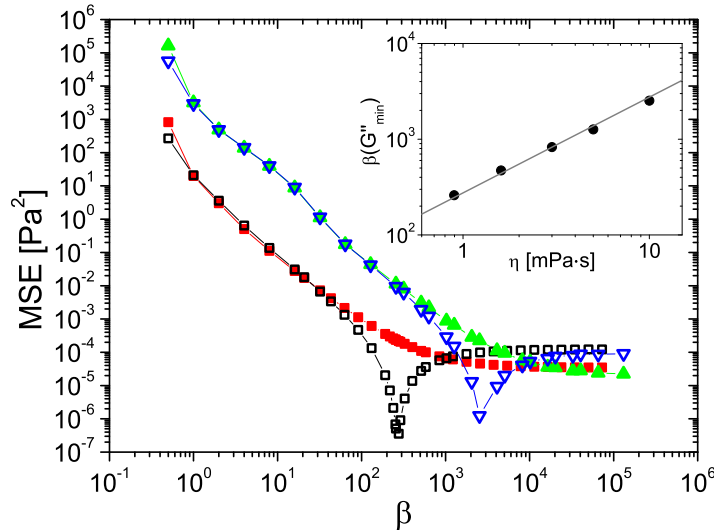$$G_{\text{tot}}^*(\omega) = \kappa/(6\pi a) + \mathrm{i}\,\eta\omega. \tag{A.7}$$

Figure 8. The mean-square error (MSE) of the viscoelastic moduli (from their expected values) versus the oversampling ratio β derived from the analysis of two NPAF having the form of a single exponential decay: $A(\tau) = e^{-\lambda\tau}$, where $\lambda = \kappa/(6\pi a\eta)$, $\kappa = 1\,\mu\text{N m}^{-1}$, $a = 2.5\,\mu\text{m}$, $\eta = 0.896\,\text{mPa s}$ (squares) and $\eta = 10\,\text{mPa s}$ (triangles), respectively. The filled and the open symbols refer to the MSE for G' and G'', respectively. The inset shows the relationship between β, taken where the MSE for G'' is minimum, and the viscosity of the Newtonian fluid (i.e. $\eta = 0.896, 1.6, 3, 5$ and $10\,\text{mPa s}$). The line is a guide for the gradient (i.e. $\beta(G''_{\text{min}}) \propto \eta$).

In summary, the LVE properties of a generic viscoelastic fluid can be obtained by subtracting the frequency-independent elastic contribution of the optical trap from equation (A.6): $G^*(\omega) = G^*_{\text{tot}}(\omega) - \kappa/(6\pi a)$; notably, this is the same expression as the one reported in equation (7), but the latter has been derived from a more rigorous analytical procedure [36, 37]. Moreover, it is important to highlight that in [36, 37], Tassieri *et al* introduced two simple experimental procedures, coupled with data analysis methods, for determining the wideband viscoelastic properties of complex fluids in measurements involving OT. Those experimental procedures are still valid as they overcame the intrinsic issue of microrheology measurements performed with static OT, i.e. the loss of information on low-frequency viscoelastic properties of fluids with relaxation times longer than t^*. In such cases, the OT compliance overshadows the fluid compliance (see figure 7) at long times (i.e. low frequencies); hence the need for either of the methods introduced in [36, 37].

Appendix B. β-parameterization of the errors

In order to better understand the implications related to the choice of the oversampling ratio β on the Fourier transform of a generic function (e.g. $A(\tau)$) via equation (9), we evaluate the MSE of the viscoelastic moduli (from their expected values) derived from the analysis of a NPAF having the form of a single exponential decay: $A(\tau) = e^{-\lambda\tau}$, where $\lambda = \kappa/(6\pi a\eta)$, as already described in the main body of the paper (e.g. see figure 1 (left)) and for which the frequency spectrum is known to have a simple analytical form (i.e. equation (A.7)).

In figure 8 we report the results obtained from the analysis of the MSE of both the moduli as a function of β for five systems differing from each other only for the viscosity values of the fluids (i.e. κ and a are kept constant, whereas $\eta = 0.896, 1.6, 3, 5$ and 10 mPa s). All five systems give similar behaviour as for the two cases shown in figure 8 (note that, not all of the curves have been shown for clarity of the graph), i.e. the MSE decreases substantially as β increases up to a value of the order of $\beta \approx 10^3$, after which it tends to stabilize around values of the order of $\approx 1E^{-5}$ and $\approx 1E^{-4}$ for G' and G'', respectively. Therefore, within a single measurement, a further increase of β above the value of $\approx 10^3$ would not induce substantial improvement of the results. Moreover, it is interesting to highlight the feature shown by the MSE curves of G'' for all five systems, i.e. they clearly exhibit a minimum before reaching the plateau at higher values of β. The inset of figure 8 shows the quasi-linear relationship between β, taken where the MSE for G'' is minimum, and the viscosity of the Newtonian fluid. The non-trivial behaviour of this error is worthy of further study.

References

[1] Ashkin A 1970 Acceleration and trapping of particles by radiation pressure *Phys. Rev. Lett.* **24** 156–9
[2] Meyer A, Marshall A, Bush B G and Furst E M 2006 Laser tweezer microrheology of a colloidal suspension *J. Rheol.* **50** 77–92
[3] Block S M, Blair D F and Berg H C 1989 Compliance of bacterial flagella measured with optical tweezers *Nature* **338** 514–8
[4] Finer J T, Simmons R M and Spudich J A 1994 Single myosin molecule mechanics: piconewton forces and nanometer steps *Nature* **368** 113–9
[5] Yoon Y-Z, Kotar J, Yoon G and Cicuta P 2008 The nonlinear mechanical response of the red blood cell *Phys. Biol.* **5** 036007
[6] Ashkin A and Dziedzic J M 1987 Optical trapping and manipulation of viruses and bacteria *Science* **235** 1517–20
[7] Tskhovrebova L, Trinick J, Sleep J A and Simmons R M 1997 Elasticity and unfolding of single molecules of the giant muscle protein titin *Nature* **387** 308–12
[8] Mehta A D, Rief M, Spudich J A, Smith D A and Simmons R M 1999 Single-molecule biomechanics with optical methods *Science* **283** 1689–95
[9] Ashkin A and Dziedzic J M 1971 Optical levitation by radiation pressure *Appl. Phys. Lett.* **19** 283–5
[10] Ashkin A, Dziedzic J M, Bjorkholm J E and Chu S 1986 Observation of a single-beam gradient force optical trap for dielectric particles *Opt. Lett.* **11** 288–90
[11] Gibson G M, Leach J, Keen S, Wright A J and Padgett M J 2008 Measuring the accuracy of particle position and force in optical tweezers using high-speed video microscopy *Opt. Express* **16** 14561–70
[12] Gittes F and Schmidt C F 1998 Interference model for back-focal-plane displacement detection in optical tweezers *Opt. Lett.* **23** 7–9
[13] Keen S, Leach J, Gibson G and Padgett M J 2007 Comparison of a high-speed camera and a quadrant detector for measuring displacements in optical tweezers *J. Opt. A: Pure Appl. Opt.* **9** S264–6
[14] Mason T G and Weitz D A 1995 Optical measurements of frequency-dependent linear viscoelastic moduli of complex fluids *Phys. Rev. Lett.* **74** 1250–3
[15] Squires T M and Mason T G 2010 Fluid mechanics of microrheology *Annu. Rev. Fluid Mech.* **42** 413–38
[16] Molloy J E and Padgett M J 2002 Lights, action: optical tweezers *Contemp. Phys.* **43** 241–58
[17] Grier D G 2003 A revolution in optical manipulation *Nature* **424** 810–6
[18] Neuman K C and Block S M 2004 Optical trapping *Rev. Sci. Instrum.* **75** 2787–809
[19] Padgett M and Leonardo R D 2011 Holographic optical tweezers and their relevance to lab on chip devices *Lab. Chip* **11** 1196–205

[20] Yao A, Tassieri M, Padgett M and Cooper J 2009 Microrheology with optical tweezers *Lab. Chip* **9** 2568–75

[21] Furst E M 2005 Applications of laser tweezers in complex fluid rheology *Curr. Opin. Colloid Interface Sci.* **10** 79–86

[22] Moffitt J R, Chemla Y R, Smith S B and Bustamante C 2008 Recent advances in optical tweezers *Annu. Rev. Biochem.* **77** 205–28

[23] Frases S, Pontes B, Nimrichter L, Rodrigues M L, Viana N B and Casadevall A 2009 The elastic properties of the Cryptococcus neoformans capsule *Biophys. J.* **97** 937–45

[24] Watts F, Tan L E, Tassieri M, McAlinden N, Wilson C G, Girkin J M and Wright A J 2011 The viscoelastic properties of the vitreous humor measured using an optically trapped local probe *Proc. SPIE* **8097** 80970H

[25] Pesce G, De Luca A C, Rusciano G, Netti P A, Fusco S and Sasso A 2009 Microrheology of complex fluids using optical tweezers: a comparison with macrorheological measurements *J. Opt. A: Pure Appl. Opt.* **11** 034016

[26] Kollmannsberger P and Fabry B 2011 Linear and nonlinear rheology of living cells *Annu. Rev. Mater. Res.* **41** 75–97

[27] Kuo S, Gelles J, Steuer E and Sheetz M 1991 *Workshop on Motor Proteins* (*Cambridge, UK, September 1990*); A model for kinesin movement from nanometer-level movements of kinesin and cytoplasmic dynein and force measurements *J. Cell Sci. Suppl.* **14** 135–8

[28] Pine D J, Weitz D A, Chaikin P M and Herbolzheimer E 1988 Diffusing-wave spectroscopy *Phys. Rev. Lett.* **60** 1134–7

[29] Weitz D A, Zhu J X, Durian D J, Gang H and Pine D J 1993 Diffusing-wave spectroscopy—the technique and some applications *Phys. Scr.* **T49B** 610–21

[30] Okajima T and Tokumoto H 2008 Nanorheology of living cells investigated by atomic force microscopy *Nihon Reoroji Gakkaishi* **36** 81–6

[31] Bausch A R, Moller W and Sackmann E 1999 Measurement of local viscoelasticity and forces in living cells by magnetic tweezers *Biophys. J.* **76** 573–9

[32] Tassieri M, Waigh T A, Trinick J, Aggeli A and Evans R M L 2010 Analysis of the linear viscoelasticity of polyelectrolytes by magnetic microrheometry-pulsed creep experiments and the one particle response *J. Rheol.* **54** 117–31

[33] Brau R R, Ferrer J M, Lee H, Castro C E, Tam B K, Tarsa P B, Matsudaira P, Boyce M C, Kamm R D and Lang M J 2007 Passive and active microrheology with optical tweezers *J. Opt. A: Pure Appl. Opt.* **9** S103–12

[34] Fischer M and Berg-Sorensen K 2007 Calibration of trapping force and response function of optical tweezers in viscoelastic media *J. Opt. A: Pure Appl. Opt.* **9** S239–50

[35] Atakhorrami M, Sulkowska J I, Addas K M, Koenderink G H, Tang J X, Levine A J, MacKintosh F C and Schmidt C F 2006 Correlated fluctuations of microparticles in viscoelastic solutions: quantitative measurement of material properties by microrheology in the presence of optical traps *Phys. Rev. E* **73** 061501

[36] Tassieri M, Gibson G M, Evans R M L, Yao A M, Warren R, Padgett M J and Cooper J M 2010 Measuring storage and loss moduli using optical tweezers: broadband microrheology *Phys. Rev. E* **81** 026308

[37] Preece D, Warren R, Evans R M L, Gibson G M, Padgett M J, Cooper J M and Tassieri M 2011 Optical tweezers: wideband microrheology *J. Opt.* **13** 044022

[38] Valentine M T, Dewalt L E and Ou-Yang H D 1996 Forces on a colloidal particle in a polymer solution: a study using optical tweezers *J. Phys.: Condens. Matter* **8** 9477–82

Valentine M T, Dewalt L E and Ou-Yang H D 1996 *3rd Conf. on Liquid Matter* (*University of East Anglia, Norwich, UK, 6–10 July*)

[39] Starrs L and Bartlett P 2003 *5th Conf. on Liquid Matter (Constance, Germany, 14–18 September)* One- and two-point micro-rheology of viscoelastic media *J. Phys.: Condens. Matter* **15** S251–6

[40] Waigh T A 2005 Microrheology of complex fluids *Rep. Prog. Phys.* **68** 685–742

[41] Pipe C J and McKinley G H 2009 Microfluidic rheometry *Mech. Res. Commun.* **36** 110–20

[42] Cicuta P and Donald A M 2007 Microrheology: a review of the method and applications *Soft Matter* **3** 1449–55

[43] Ferry J D 1980 *Viscoelastic Properties of Polymers* 3rd edn (New York: Wiley)

[44] Hasan S W, Ghannam M T and Esmail N 2010 Heavy crude oil viscosity reduction and rheology for pipeline transportation *Fuel* **89** 1095–100

[45] Stokes J R and Davies G A 2007 Viscoelasticity of human whole saliva collected after acid and mechanical stimulation *Biorheology* **44** 141–60

[46] Gittes F, Schnurr B, Olmsted P D, MacKintosh F C and Schmidt C F 1997 Microscopic viscoelasticity: shear moduli of soft materials determined from thermal fluctuations *Phys. Rev. Lett.* **79** 3286–9

[47] Mason T G, Ganesan K, van Zanten J H, Wirtz D and Kuo S C 1997 Particle tracking microrheology of complex fluids *Phys. Rev. Lett.* **79** 3282–5

[48] Buchanan M, Atakhorrami M, Palierne J F and Schmidt C F 2005 Comparing macrorheology and one- and two-point microrheology in wormlike micelle solutions *Macromolecules* **38** 8840–4

[49] Crocker J C, Valentine M T, Weeks E R, Gisler T, Kaplan P D, Yodh A G and Weitz D A 2000 Two-point microrheology of inhomogeneous soft materials *Phys. Rev. Lett.* **85** 888–91

[50] Savin T and Doyle P S 2005 Static and dynamic errors in particle tracking microrheology *Biophys. J.* **88** 623–38

[51] Mason T G 2000 Estimating the viscoelastic moduli of complex fluids using the generalized Stokes–Einstein equation *Rheol. Acta* **39** 371–8

[52] Dasgupta B R, Tee S-Y, Crocker J C, Frisken B J and Weitz D A 2002 Microrheology of polyethylene oxide using diffusing wave spectroscopy and single scattering *Phys. Rev.* E **65** 051505

[53] Yanagishima T, Frenkel D, Kotar J and Eiser E 2011 Real-time monitoring of complex moduli from micro-rheology *J. Phys.: Condens. Matter* **23** 194118

[54] Evans R M L, Tassieri M, Auhl D and Waigh T A 2009 Direct conversion of rheological compliance measurements into storage and loss moduli *Phys. Rev.* E **80** 012501

[55] Gibson G M, Leach J, Keen S, Wright A J and Padgett M J 2008 Measuring the accuracy of particle position and force in optical tweezers using high-speed video microscopy *Opt. Express* **16** 14561–70

[56] Berg-Sorensen K and Flyvbjerg H 2004 Power spectrum analysis for optical tweezers *Rev. Sci. Instrum.* **75** 594–612

[57] Tolić-Nørrelykke S F, Schäffer E, Howard J, Pavone F S, Jülicher F and Flyvbjerg H 2006 Calibration of optical tweezers with positional detection in the back focal plane *Rev. Sci. Instrum.* **77** 103101

[58] Evans R M L 2009 Transforming from time to frequency without artefacts *Br. Soc. Rheol. Bull.* **50** 76

[59] Spruijt E, Sprakel J, Lemmers M, Cohen Stuart M A and van der Gucht J 2010 Relaxation dynamics at different time scales in electrostatic complexes: time-salt superposition *Phys. Rev. Lett.* **105** 208301

[60] Shannon C E 1949 Communication in the presence of noise *Proc. IRE* **37** 10–21

[61] Lathi B P 2004 *Linear Systems and Signals* (*Oxford Series in Electrical and Computer Engineering*) (Oxford: Oxford University Press)

[62] Wu P, Huang R, Tischer C, Jonas A and Florin E-L 2009 Direct measurement of the nonconservative force field generated by optical tweezers *Phys. Rev. Lett.* **103** 108101

[63] Pesce G, Volpe G, De Luca A C, Rusciano G and Volpe G 2009 Quantitative assessment of non-conservative radiation forces in an optical trap *Europhys. Lett.* **86** 38002

[64] Franosch T, Grimm M, Belushkin M, Mor F M, Foffi G, Forró L and Jeney S 2011 Resonances arising from hydrodynamic memory in Brownian motion *Nature* **478** 85–8

[65] Jannasch A, Mahamdeh M and Schäffer E 2011 Inertial effects of a small Brownian particle cause a colored power spectral density of thermal noise *Phys. Rev. Lett.* **107** 228301

[66] Tassieri M, Evans R M L, Barbu-Tudoran L, Trinick J and Waigh T A 2008 The self-assembly, elasticity and dynamics of cardiac thin filaments *Biophys. J.* **94** 2170–8

[67] Tassieri M, Evans R M L, Barbu-Tudoran L, Nasir Khaname G, Trinick J and Waigh T A 2008 Dynamics of semiflexible polymer solutions in the highly entangled regime *Phys. Rev. Lett.* **101** 198301

[68] Addas K M, Schmidt C F and Tang J X 2004 Microrheology of solutions of semiflexible biopolymer filaments using laser tweezers interferometry *Phys. Rev.* E **70** 021503

[69] Schnurr B, Gittes F, MacKintosh F C and Schmidt C F 1997 Determining microscopic viscoelasticity in flexible and semiflexible polymer networks from thermal fluctuations *Macromolecules* **30** 7781–92

[70] Holmes K C, Popp D, Gebhard W and Kabsch W 1990 Atomic model of the actin filament *Nature* **347** 44–9

[71] Isambert H, Venier P, Maggs A C, Fattoum A, Kassab R, Pantaloni D and Carlier M F 1995 Flexibility of actin-filaments derived from thermal fluctuations—effect of bound nucleotide, phalloidin and muscle regulatory proteins *J. Biol. Chem.* **270** 11437–44

[72] Gittes F, Mickey B, Nettleton J and Howard J 1993 Flexural rigidity of microtubules and actin-filaments measured from thermal fluctuations in shape *J. Cell Biol.* **120** 923–34

[73] Gotter R, Kroy K, Frey E, Barmann M and Sackmann E 1996 Dynamic light scattering from semidilute actin solutions: a study of hydrodynamic screening, filament bending stiffness and the effect of tropomyosin/troponin-binding *Macromolecules* **29** 30–6

[74] Mackintosh F C, Käs J and Janmey P A 1995 Elasticity of semiflexible biopolymer networks *Phys. Rev. Lett.* **75** 4425–8

[75] Farge E and Maggs A C 1993 Dynamic scattering from semiflexible polymers *Macromolecules* **26** 5041–4

[76] Morse D C 1998 Viscoelasticity of concentrated isotropic solutions of semiflexible polymers. 2. Linear response *Macromolecules* **31** 7044–67

[77] Everaers R, Julicher F, Ajdari A and Maggs A C 1999 Dynamic fluctuations of semiflexible filaments *Phys. Rev. Lett.* **82** 3717–20

[78] Liverpool T B and Maggs A C 2001 Dynamic scattering from semiflexible polymers *Macromolecules* **34** 6064–73

[79] Hiraiwa T and Ohta T 2009 Viscoelasticity of a single semi flexible polymer chain *Macromolecules* **42** 7553–62

[80] Obermayer B and Frey E 2009 Tension dynamics and viscoelasticity of extensible wormlike chains *Phys. Rev.* E **80** 040801

[81] Xu J Y, Viasnoff V and Wirtz D 1998 Compliance of actin filament networks measured by particle-tracking microrheology and diffusing wave spectroscopy *Rheol. Acta* **37** 387–98